Radial Exchange Density and Electron Delocalization in Molecules

Jens Geier*

Albert-Ludwigs-Universität, Institut für Organische Chemie und Biochemie, Albertstraβe 21, D-79104 Freiburg i. Br., Germany

Received: January 9, 2008; Revised Manuscript Received: February 26, 2008

The six-dimensional exchange density $\Gamma_X(\mathbf{r}_1,\mathbf{r}_2)$ is a measure of electron delocalization at the Hartree−Fock level. Fixation of $\mathbf{r}_1$ to a constant point results in a three-dimensional function, which displays electron delocalization that originates from $\mathbf{r}_1$ in position space. In this work, the dimensionality of $\Gamma_X(\mathbf{r}_1,\mathbf{r}_2)$ is lowered from six to four by integration with regard to $\mathbf{r}_2$ over sphere surfaces of radius d, centered at $\mathbf{r}_1 = \mathbf{r}$. The resulting radial exchange density $\Gamma_X(d,\mathbf{r})$ is visualized for constant d values as a function of $\mathbf{r}$. This approach indicates regions of position space which are origins of delocalization over a certain distance d. The shape of these regions very strongly depends on d. Structures similar to π orbital densities are observed at large d values (4.5 au) in unsaturated carbon compounds, while smaller values (1.5 au) can result in structures, which resemble the Laplacian of the electron density. The abundance of different spatial structures inherent in the radial exchange density implies interesting capabilities for the orbital-independent interpretation of electronic structures in position space.

Introduction

Visualization of atomic or molecular electronic structures is generally a formidable task, because of the high dimensionality of the wavefunction Ψ and its associated density matrix $\Psi\Psi^*$. Integration of $\Psi\Psi^*$ with regard to $N - 1$ sets of space and spin coordinates (N: number of electrons) yields after multiplication with N the first-order reduced density matrix, whose spin-integrated diagonal element is the electron density $\rho(\mathbf{r})$. This three-dimensional function is easily visualized in real physical space (position space) and has also a clear meaning: $\rho(\mathbf{r})dv$ equals N times the probability of finding an electron in volume dv around space point $\mathbf{r}$.[1,2] Its topology provides the basis for the quantum mechanical definition of atoms in molecules (QTAIM).[3–5] Local concentrations in $\rho(\mathbf{r})$, which can be detected in its Laplacian $\nabla^2\rho(\mathbf{r})$, indicate spatial regions where increased electron localization takes place.[6–10] Other three-dimensional functions, which are employed for related purposes, are the electron localization function (ELF),[11–14] the electron localizability indicator (ELI),[15–17] and the localized orbital locator (LOL).[18] It is also possible to determine spatial domains, which maximize the probability of containing a given number of electrons.[19] The description of electron delocalization between two points $\mathbf{r}_1$ and $\mathbf{r}_2$, a nonlocal property, requires functions $f(\mathbf{r}_1,\mathbf{r}_2)$ with explicit dependence on six space coordinates, like the exchange density $\Gamma_X(\mathbf{r}_1,\mathbf{r}_2)$,[20,21] the exchange-correlation density $\Gamma_{XC}(\mathbf{r}_1,\mathbf{r}_2)$,[22,23] and the sharing index $I(\mathbf{r}_1,\mathbf{r}_2)$.[24,25] For visualization and comprehension of such functions, it is necessary to lower their dimensionality, while preserving the nonlocal information content. One may, for example, fix the three $\mathbf{r}_1$ coordinates (or integrate them over a finite region V) and evaluate f along the $\mathbf{r}_2$ coordinates. This procedure reveals the three-dimensional structure of delocalization that originates from $\mathbf{r}_1$ (or the region V). Another possibility is to substitute $\mathbf{r}_2$ with $(\mathbf{r}_1 + \mathbf{d})$ and integrate $f(\mathbf{r}_1,\mathbf{r}_1 + \mathbf{d})$ with regard to $\mathbf{r}_1$ over the entire space. The resulting function $f_1(\mathbf{d})$ measures the total delocalization between all pairs of points that are separated by the vector $\mathbf{d}$. It is a three-dimensional function, but because it is defined in the space of distance vectors, it cannot be directly mapped on molecular structures. Additional angular integration of $f_1(\mathbf{d})$ yields a one-dimensional function $f_2(d)$, which gives the total delocalization over a distance d, independent from direction. The resolution of $f_2(d)$ into position space contributions, that is, investigation of a four-dimensional function $f_3(d,\mathbf{r})$, which measures at each point $\mathbf{r}$ the total delocalization from $\mathbf{r}$ over all other points located in a distance d from $\mathbf{r}$, constitutes the subject of this paper. The exchange density $\Gamma_X(\mathbf{r}_1,\mathbf{r}_2)$ is chosen as $f(\mathbf{r}_1,\mathbf{r}_2)$, hence the functions $f_1(\mathbf{d})$, $f_2(d)$, and $f_3(d,\mathbf{r})$ are equal to the exchange intracule density times two, $2K(\mathbf{d})$,[26–28] the radial exchange intracule density (radial K-intracule density) times two, $2K(d)$,[26,27] and the radial exchange density $\Gamma_X(d,\mathbf{r})$. Evaluation of $\Gamma_X(d,\mathbf{r})$ along $\mathbf{r}$ for several fixed d values reveals interesting spatial aspects of electronic structures, because the predominant delocalization distances vary strongly with the position in a molecule. The shapes of the spatial domains appearing at certain d values are often qualitatively interpretable in terms of chemical objects and concepts like single, double, or triple bonds, lone pairs, and bond conjugation.

Theory. Electron delocalization between two space points $\mathbf{r}_1$ and $\mathbf{r}_2$ is defined at the Hartree−Fock (HF) level through the exchange density $\Gamma_X(\mathbf{x}_1,\mathbf{x}_2)$,[21,23] which is the correlated part of the HF electron pair density $\Gamma(\mathbf{x}_1,\mathbf{x}_2)$ ($\mathbf{x}_i$ denotes combined space-spin coordinates $\mathbf{r}_i$, s_i):[1,2,29]

$$\Gamma(\mathbf{x}_1,\mathbf{x}_2) = \frac{1}{2}[\rho(\mathbf{x}_1)\rho(\mathbf{x}_2) + \Gamma_X(\mathbf{x}_1,\mathbf{x}_2)] \qquad (1)$$

$\Gamma(\mathbf{x}_1,\mathbf{x}_2)dv_1dv_2$ gives the probability of finding an electron with spin s_1 in volume dv_1 around $\mathbf{r}_1$ and another one with spin s_2 in volume dv_2 around $\mathbf{r}_2$, multiplied by the number of distinct electron pairs. The total number of distinct pairs, which can be formed from a set of N electrons is $\frac{1}{2}N(N-1) = \frac{1}{2}(N^2 - N)$.[1] The uncorrelated product of electron densities $\rho(\mathbf{x}_1)\rho(\mathbf{x}_2)$

* Corresponding author. E-mail: geier@ocbc.uni-freiburg.de.

10.1021/jp800202w CCC: $40.75
Published on Web 05/20/2008

integrates to N^2 instead of the correct number of $N(N\text{-}1)$, because it contains N fictitious self-pairs,[21] which are removed in equation 1 by the exchange density $\Gamma_X(\mathbf{x}_1,\mathbf{x}_2)$. The exchange density describes electron correlation due to the Pauli principle (Fermi correlation). It is always lower than or equal to zero and integrates to $-N$:

$$\int\int \Gamma_X(\mathbf{x}_1,\mathbf{x}_2)\, d\mathbf{x}_2 d\mathbf{x}_1 = -\int \rho(\mathbf{x}_1) d\mathbf{x}_1 = -N \qquad (2)$$

$\Gamma_X(\mathbf{x}_1,\mathbf{x}_2)$ can hence be interpreted as self-pair density, that is, as a quantitative measure of electron delocalization.[6,20,30,31] High absolute values of $\Gamma_X(\mathbf{x}_1,\mathbf{x}_2)$ correspond to strong delocalization between position space points $\mathbf{r}_1$ and $\mathbf{r}_2$. $\Gamma_X(\mathbf{x}_1,\mathbf{x}_2)$ is the negative of the squared absolute value of the first-order reduced density matrix $\gamma(\mathbf{x},\mathbf{x}')$:

$$\Gamma_X(\mathbf{x}_1,\mathbf{x}_2) = -|\gamma(\mathbf{x}_1,\mathbf{x}_2)|^2 = -\gamma(\mathbf{x}_1,\mathbf{x}_2)\gamma(\mathbf{x}_2,\mathbf{x}_1) \qquad (3)$$

Integration of the spin coordinates partitions $\Gamma_X(\mathbf{x}_1,\mathbf{x}_2)$ in two components, which are given in terms of the spatial parts of molecular spin orbitals φ as:

$$\begin{aligned}\Gamma_X(\mathbf{r}_1,\mathbf{r}_2) &= \int \Gamma_X(\mathbf{x}_1,\mathbf{x}_2)\, ds_1 ds_2 \\ &= \Gamma_X^{\alpha\alpha}(\mathbf{r}_1,\mathbf{r}_2) + \Gamma_X^{\beta\beta}(\mathbf{r}_1,\mathbf{r}_2) \\ &= -\left|\sum_i^{\alpha} \phi_i^{\alpha}(\mathbf{r}_1)\phi_i^{\alpha}(\mathbf{r}_2)^*\right|^2 - \left|\sum_i^{\beta} \phi_i^{\beta}(\mathbf{r}_1)\phi_i^{\beta}(\mathbf{r}_2)^*\right|^2\end{aligned} \qquad (4)$$

At post-HF levels $\Gamma_X(\mathbf{x}_1,\mathbf{x}_2)$ in equation 1 is replaced with the exchange-correlation density $\Gamma_{XC}(\mathbf{x}_1,\mathbf{x}_2)$, which includes additionally the effects of Coulomb correlation and hence contains also unlike-spin components [$\Gamma_{XC}(\mathbf{r}_1,\mathbf{r}_2) = \Gamma_{XC}^{\alpha\alpha}(\mathbf{r}_1,\mathbf{r}_2) + \Gamma_{XC}^{\alpha\beta}(\mathbf{r}_1,\mathbf{r}_2) + \Gamma_{XC}^{\beta\alpha}(\mathbf{r}_1,\mathbf{r}_2) + \Gamma_{XC}^{\beta\beta}(\mathbf{r}_1,\mathbf{r}_2)$].[23] Integration of $-\Gamma_X(\mathbf{r}_1,\mathbf{r}_2)$ or $-\Gamma_{XC}(\mathbf{r}_1,\mathbf{r}_2)$ respectively with regard to $\mathbf{r}_1$ and $\mathbf{r}_2$ over finite three-dimensional regions V_i and V_j gives the number of electrons which are localized within a region ($V_i = V_j$) or the number of electrons which are delocalized from V_i over V_j ($V_i \neq V_j$). In the case of atomic basins B as regions V, these numbers correspond to the localization index $\lambda(B_i)$ or half times the delocalization index $\delta(B_i,B_j)$[22,30,32–39] (which is equal to the shared electron distribution index, SEDI[40,41]). The difference between an atomic electron population $\bar{N}(B_i)$ and the localization index $\lambda(B_i)$ equals the variance of $N(B_i)$, while $-\delta(B_i,B_j)/2$ are its covariances[31,39,42,43] (for the relation between variances of electron populations and electron localization, cf. also refs 44–46). The pattern of delocalization indicated by $\delta(B_i,B_j)$ is usually in accord with qualitative resonance theory. Methods for the determination of real space resonance structures (based on the QTAIM partitioning), into whose contributions $\delta(B_i,B_j)$ can be decomposed, have recently been developed.[47–49] The relation between delocalization and resonance structures has also been extensively discussed by means of the natural polyelectron population analysis,[50–53] which involves the representation of the wavefunction by Slater determinants built from natural atomic orbitals. The inclusion of Coulomb correlation by means of CI or CASSCF calculations leads in most cases (except ionic closed-shell interactions) to smaller delocalization indices than those obtained by the HF method.[22,30,41,54] A heuristic replacement of the HF orbitals in equation 4 by Kohn−Sham orbitals[55] from B3LYP calculations is possible but does not introduce the effects of Coulomb correlation.[22,56] Usually the delocalization indices obtained with B3LYP orbitals are somewhat larger than the HF values.

Unlike the HF exchange density, the exchange-correlation density $\Gamma_{XC}(\mathbf{r}_1,\mathbf{r}_2)$ at post-HF levels is not a pure self-pair density. This is obvious for its unlike-spin components (which can be positive or negative and integrate to zero over entire space), but also its like-spin components include Coulomb correlation besides the dominant exchange correlation and can hence adopt local positive values[57] (over entire space they integrate to the negative number of electrons). There exist also other definitions of electron delocalization, which coincide for single determinant wavefunctions with the HF exchange density (or its absolute value, respectively). A quantity, which is defined analogously to $\Gamma_X(\mathbf{x}_1,\mathbf{x}_2)$ in equation 3, but with the correlated instead of the HF first-order reduced density matrix, has been proposed for the evaluation of bond orders.[58,59] Unlike the HF exchange density, this quantity does not integrate to the negative number of electrons. Substitution of the eigenvalues n_i (occupation numbers) of $\gamma(\mathbf{x},\mathbf{x}')$ by their positive square roots leads to a function which integrates to $-N$ and which has been proposed as an approximation to the exact $\Gamma_{XC}(\mathbf{r}_1,\mathbf{r}_2)$ (φ: spatial parts of natural spin orbitals):[23,36,60]

$$\begin{aligned}\Gamma_{XC}^{approx}(\mathbf{r}_1,\mathbf{r}_2) = &-\left|\sum_i^{\alpha} \sqrt{n_i^{\alpha}}\phi_i^{\alpha}(\mathbf{r}_1)\phi_i^{\alpha}(\mathbf{r}_2)^*\right|^2 \\ &-\left|\sum_i^{\beta} \sqrt{n_i^{\beta}}\phi_i^{\beta}(\mathbf{r}_1)\phi_i^{\beta}(\mathbf{r}_2)^*\right|^2\end{aligned} \qquad (5)$$

In contrast to the exact $\Gamma_{XC}(\mathbf{r}_1,\mathbf{r}_2)$, this function is always lower than or equal to zero, and it does not satisfy the Pauli exclusion principle. The same quantity, with an inverted sign, has been derived as a measure of electron delocalization using arguments based solely on the first-order reduced density matrix and is termed sharing index $I(\mathbf{r}_1,\mathbf{r}_2)$.[24,25,61–64] In the present work, the HF level (i.e. $n_i^{\alpha},n_i^{\beta} = 1$ for all i) is employed throughout; hence, all definitions lead to the same results.

As a six-dimensional function, $\Gamma_X(\mathbf{r}_1,\mathbf{r}_2)$ contains an enormous amount of information. A straightforward way to investigate its structure is by fixing $\mathbf{r}_1$ to a certain location and evaluating $\Gamma_X(\mathbf{r}_1,\mathbf{r}_2)$ (or the related Fermi hole density $\Gamma_X^{\sigma\sigma}(\mathbf{r}_1,\mathbf{r}_2)/\rho^{\sigma}(\mathbf{r}_1)$; σ, spin label) along $\mathbf{r}_2$ in three-dimensional position space.[20,65–69] Because the number of different $\mathbf{r}_1$ points, which have to be considered in order to obtain a coarse overview of its structure, can be quite high, it is convenient to integrate $\mathbf{r}_1$ over a finite three-dimensional region, especially an atomic basin B. The resulting atomic exchange density $\Gamma_X(B;\mathbf{r})$ ($\mathbf{r} = \mathbf{r}_2$) represents after sign inversion the delocalization of the electron population of the basin B. $\Gamma_X(B;\mathbf{r})$ is a special case of the domain-averaged Fermi hole (DAFH)[70–72] (DAFH's are the starting points for a bonding analysis which is based on the eigenvalues and eigenfunctions of their matrix representations[72]). In the case of small molecules, the integration of $\mathbf{r}_1$ over a whole atomic basin is however of limited use, because many of the most interesting structures of $\Gamma_X(B;\mathbf{r})$ appear usually outside the integration basin and the basins of the directly adjacent atoms; that is, they are associated with long-range delocalization.[73] Structural details within or in the vicinity of the integration basin are easier to recognize in the Laplacian of $\Gamma_X(B;\mathbf{r})$.[73]

Instead of considering the whole range of delocalization that originates from a single reference point or basin, one may examine the total amount of delocalization from a reference point over a certain distance in dependence of the location of the reference point. This means to integrate $\Gamma_X(\mathbf{r}_1,\mathbf{r}_2)$ with regard to $\mathbf{r}_2$ over the surface of a sphere with radius d centered at $\mathbf{r}_1 = \mathbf{r}$, that is, to form the radial exchange density $\Gamma_X(d,\mathbf{r})$ (d, $\Omega_{\mathbf{d}}$: radius and solid angle of vector $\mathbf{d}$):

$$\Gamma_X(d,\mathbf{r}) = d^2 \int \Gamma_X(\mathbf{r},\mathbf{r}+\mathbf{d})\, d\Omega_d \quad (6)$$

Further integration of $\Gamma_X(d,\mathbf{r})$ with regard to d from 0 to ∞ gives the negative electron density at $\mathbf{r}$ (cf. eq 2), while integration with regard to $\mathbf{r}$ over entire space yields two times the radial K-intracule density $K(d)$,[26,27] which is the exchange part of the radial intracule density $P(d)$[26,27,74–77] at the HF level. The intracule density $I(\mathbf{d})$, from which $P(d)$ is derived by angular integration, is the probability density for finding two electrons separated by the vector $\mathbf{d}$:[26,27,78]

$$I(\mathbf{d}) = \int \Gamma(\mathbf{r},\mathbf{r}+\mathbf{d})\, d\mathbf{r} \quad (7)$$

The exchange part of the HF intracule density is $\frac{1}{2}\int \Gamma_X(\mathbf{r},\mathbf{r}+\mathbf{d})d\mathbf{r}$ (cf. equation 1), hence:

$$K(d) = d^2 \int \left[\frac{1}{2}\int \Gamma_X(\mathbf{r},\mathbf{r}+\mathbf{d})\, d\mathbf{r}\right] d\Omega_d = \frac{1}{2}\int \Gamma_X(d,\mathbf{r})\, d\mathbf{r} \quad (8)$$

The topologies of the intracule density[28,79–82] and its Laplacian[83,84] have been investigated for molecular systems and found to contain a wealth of relevant electronic structure information. The radial intracule density $P(d)$ is of special interest because it can also be obtained experimentally from X-ray and electron scattering intensities.[85–87]

$\Gamma_X(d,\mathbf{r})$ is an interesting mathematical device for visualizing nonlocal features of molecular electronic structures, especially when it is evaluated for fixed d values along $\mathbf{r}$, as will be shown below. The structures of related spherically averaged hole densities have been discussed for atoms.[88,89] Furthermore, a Taylor expansion has been derived for the spherically averaged exchange charge density, which is $\Gamma_X^{\sigma\sigma}(d,\mathbf{r})$ divided by $-4\pi d^2\rho^\sigma(\mathbf{r})$.[90] Nonlocal electronic properties have also been investigated in the structures of the first-order reduced density matrix $\gamma(\mathbf{r},\mathbf{r}')$[91–93] and the parity function,[18,94,95] which is defined as $\int\gamma(\mathbf{r}-\mathbf{s},\mathbf{r}+\mathbf{s})\, d\mathbf{s}$. A decomposition of $\gamma(\mathbf{r},\mathbf{r}')$ into local contributions forms the basis of the natural resonance theory[96] (which must not be confused with the natural polyelectron analysis cited above). Finally, a different approach for the position space analysis of electron delocalization should be mentioned, which relies on the anisotropy of the induced current density.[97]

Computational Details. The structures of molecules **1**−**10** were optimized[98] with the Gaussian 03 program[99] at the B3LYP/6-311++G(2d,2p) level. They represent minima according to their Hessian eigenvalues. Molecular orbitals were obtained in wfn file format (program keywords: 6d 10f, output = wfn) from single point HF/6-311++G(2d,2p) calculations at the B3LYP/6-311++G(2d,2p) geometries. A Fortran program, which uses wfn files as input, was employed for the calculation of the radial exchange density from the HF orbitals according to eqs 4 and 6 over a cubic grid. The resulting values were saved in cube file format.[100] Grid intervals of 0.10 (molecules **1**−**5**, **9**) and 0.15 au (**6**–**8**, **10**) were employed. Isosurface representations and contour line diagrams were generated from the cube files with the program Molekel.[101]

The integration of the exchange density over sphere surfaces[102] was performed numerically using angular grids derived from extremal fundamental systems of points.[103,104] These grids have good geometric properties and are available up to a size of 36 864 points (degree 191).[103] Integration performance was checked by comparison of the $\Gamma_X(d,\mathbf{r})$ values obtained from different grids at several thousand (or hundreds of thousands in the case of **1** to **5**) test locations $\mathbf{r}$, which were distributed uniformly over the molecule (i.e. at the nodes of a cubic lattice, extending up to 2 au distance from the outermost nuclei). The values obtained with 10 000 angular points for $d = 6.0$ and 4.5 au, 7225 points for $d = 3.0$, 2.5, and 2.0 au, and 5776 points for $d = 1.5$, 1.0, and 0.5 au differ by less than $\pm 1 \times 10^{-5}$ au from the values obtained with the 36 864 grid at more than 98% of the test locations (within the same range of accuracy, the values are invariant to grid rotations). The rotation invariance of the values obtained from the 36 864 grid is better than $\pm 1 \times 10^{-6}$ au at >98% of the test locations; the exceptions occur mainly when the exchange density spreads significantly over an inner atomic core region, which is intersected by the integration sphere surface (the accuracy may then drop to approximately $\pm 1 \times 10^{-4}$ au). The 36 864-grid values were further verified at selected locations by comparison with the values obtained from more time-consuming product quadratures in θ and φ angles (Gauss−Chebychev formulas of second kind/trapezoidal rule[105]). Despite larger sphere areas, the integrations for $d = 4.5$ and 6.0 au were generally found to converge easier than those for $d = 1.5$ to 2.5 au, indicating that contributions from the core regions become less important with larger distances d. The final calculations for molecules **6**–**10** were performed with the 10 000 ($d = 6.0$ and 4.5 au), 7225 ($d = 3.0$, 2.5, and 2.0 au), and 5776 grids ($d = 1.5$, 1.0, and 0.5 au), while in the case of the smaller systems **1**–**5** the 36 864 grid was used for all radii. In any case, the attained mean accuracy is sufficient for the determination of the contour lines and isosurfaces employed in this work.

Delocalization indices and atomic electron populations were obtained with the AIM2000 program[106,107] (the absolute values of the integrals of $L = -\frac{1}{4}\nabla^2\rho(\mathbf{r})$ over atomic basins were smaller than 5×10^{-4} au in all cases).

Results and Discussion

The structure of the radial exchange density is discussed in the following for several carbon-containing molecules, which feature different kinds of chemical bonding and conjugation. $\Gamma_X(d,\mathbf{r})$ is visualized as a function of $\mathbf{r}$ for different fixed d values, which are chosen as multiples of 0.5 au (1 Bohr = 0.529177 Å). Because $\Gamma_X(d,\mathbf{r})$ is necessarily less than or equal to zero (cf. equation 3), descriptive notions like "accumulation" and "thinning" can be used without sign specification and refer here to its absolute values. The radial exchange density of ethylene **1** (D_{2h}; d(C−C) = 1.326 Å = 2.505 au) is shown in Figures 1 and 2.

At a small delocalization radius d of 0.5 au (Figure 1a−d), $\Gamma_X(d,\mathbf{r})$ appears as a weakly structured function, which accumulates mainly with approximately spherical shape in the inner regions of the carbon atoms (the same holds also at smaller values of d, i.e., at $d = 0.4$, 0.3, 0.2, and 0.1 au). In this regard, it resembles the electron density $\rho(\mathbf{r})$. Similarities to the latter are expected for very small delocalization radii because, in the case of sufficiently small $\mathbf{d}$, the exchange density $\Gamma_X^{\sigma\sigma}(\mathbf{r},\mathbf{r}+\mathbf{d})$ behaves approximately like $-\rho^\sigma(\mathbf{r})\rho^\sigma(\mathbf{r}+\mathbf{d})$ (this relation implies that $\mathbf{r}$ and $\mathbf{r}+\mathbf{d}$ are both located inside a region which can be approximated as the spatial part of a single localized orbital);[23,65,88] for $\mathbf{d} = \mathbf{0}$ the relation is exact, compare with eq 4.

Upon increasing the delocalization radius to 1.0 au (Figure 1 e−h), the structure of $\Gamma_X(d,\mathbf{r})$ changes markedly. In $\Gamma_X(1.0,\mathbf{r})$, the carbon nuclei are located in thinned out regions, while there appear five new prolate accumulation domains (Figure 1f,h), which surround the C−H and C−C bonds. It is of interest, here, that the core loge[31] of the carbon atom in methane, a spherical region, centered at the nucleus position, which exhibits a

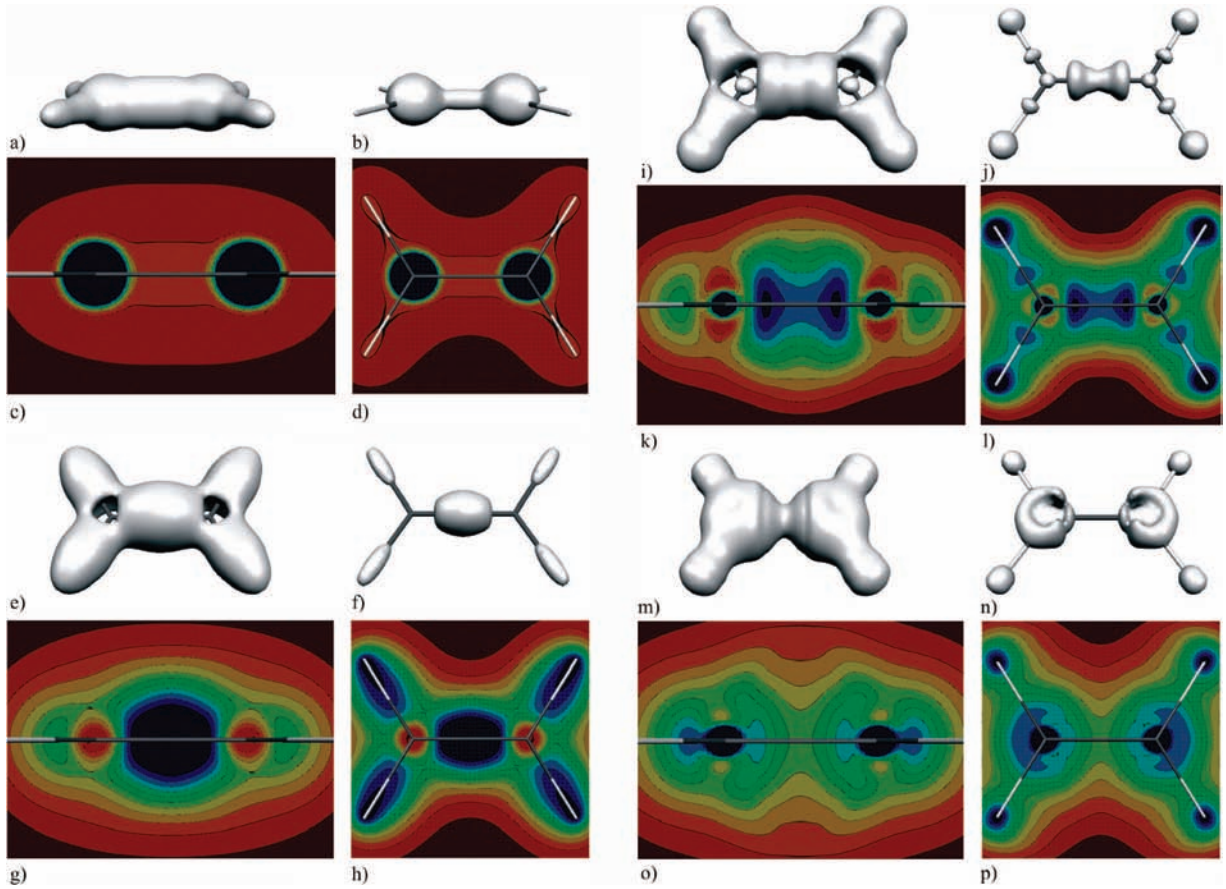

Figure 1. Radial exchange density in ethylene **1**. a,b,e,f,i,j,m,n: Isosurface representations. c,d,g,h,k,l,o,p: Contour line diagrams in planes containing both carbon nuclei, perpendicular (c,g,k,o) and parallel (d,h,l,p) to the molecular plane. Contour line values decrease in constant steps from the outer boundary of the red zone (starting value) in the direction red → yellow → green → blue. (a) $\Gamma_X(0.5,\mathbf{r}) = -0.09$ au. (b) $\Gamma_X(0.5,\mathbf{r}) = -0.15$ au. (c,d) $\Gamma_X(0.5,\mathbf{r})$: starting value $= -0.01$ au, step size $= 0.1$ au. (e) $\Gamma_X(1.0,\mathbf{r}) = -0.11$ au. (f) $\Gamma_X(1.0,\mathbf{r}) = -0.2$ au. (g,h) $\Gamma_X(1.0,\mathbf{r})$: starting value $= -0.01$ au, step size $= 0.02$ au. (i) $\Gamma_X(1.5,\mathbf{r}) = -0.11$ au. (j) $\Gamma_X(1.5,\mathbf{r}) = -0.15$ au. (k,l) $\Gamma_X(1.5,\mathbf{r})$: starting value $= -0.03$ au, step size $= 0.015$ au. (m) $\Gamma_X(2.0,\mathbf{r}) = -0.05$ au. (n) $\Gamma_X(2.0,\mathbf{r}) = -0.08$ au. (o,p) $\Gamma_X(2.0,\mathbf{r})$: starting value $= -0.01$ au, step size $= 0.01$ au.

minimum of external delocalization and contains in the average 2.01 electrons, has a radius of 0.53 au.[31,61] Assuming a similar core loge radius for the ethylene carbon atoms, it follows that for most locations of **r** within the loge the associated integration sphere surface is with $d = 1.0$ au completely outside. This may be one of the factors responsible for the thinning of $\Gamma_X(1.0,\mathbf{r})$ in vicinity of the carbon nuclei. The main characteristic of $\Gamma_X(1.0,\mathbf{r})$ is accumulation between adjacent atomic centers. This feature persists when d is raised to 1.5 au, a value which corresponds to about half the C−C bond length (Figure 1). Therefore, $\Gamma_X(1.5,\mathbf{r})$ and $\Gamma_X(1.0,\mathbf{r})$ are grouped into the same delocalization range (which may be denoted as proximal delocalization). However, each of the five accumulation domains of $\Gamma_X(1.0,\mathbf{r})$ is split in two new ones in $\Gamma_X(1.5,\mathbf{r})$. In addition, there occurs again accumulation in the vicinity of the carbon nuclei. It should be noted that the structure of $\Gamma_X(1.5,\mathbf{r})$ appears here and also in other cases (vide infra), similar to that of the negative value range of the Laplacian of the electron density $\nabla^2\rho(\mathbf{r})$.[6]

Upon increasing d to 2.0 au, the accumulation between the carbon centers disappears. By virtue of this structural difference, $\Gamma_X(2.0,\mathbf{r})$ (Figure 1m−p) is assigned to the next delocalization range, which covers C−H and C−C bond distances and can hence be denoted as vicinal or 1,2-delocalization. The complicated shape of $\Gamma_X(2.0,\mathbf{r})$ at the carbon atoms reflects the transition from the spatially strongly structured regions, which are responsible for proximal delocalization over $d = 1.5$ au, to the relatively simple structured regions which are the origins of delocalization over $d = 2.5$ au (Figure 2a−d), a value close to the C−C bond length of 2.505 au.

The thinned out regions of $\Gamma_X(1.5,\mathbf{r})$ at the carbon atoms, which appear above and below the plane of the nuclei (Figure 1k), are still recognizable in $\Gamma_X(2.0,\mathbf{r})$, for example, as indentations in the isosurface for −0.08 au (Figure 1n). $\Gamma_X(2.0,\mathbf{r})$ shows stronger accumulation near the hydrogen nuclei than $\Gamma_X(2.5,\mathbf{r})$, because the corresponding delocalization radius is closer to the C−H bond length of 2.045 au (1.082 Å) than in the latter case.

At none of the d values considered so far appear any clear indications for the presence of π delocalization between the doubly bonded carbon atoms. It is however to be expected that structures resembling π orbital densities occur at larger values of d, because at least in one direction, perpendicular to the molecular plane, π orbitals have a larger spatial extension than σ orbitals. Their contribution along the integration area should thus become more important relative to the latter at large sphere radii. Further, due to the smaller number of occupied π molecular orbitals, these exhibit less sign alternations and consequently less destructive interference (cf. equation 4) than σ orbitals. The first π orbital density-like features are already apparent at $d = 3.0$ au (Figure 2e−h), where two additional accumulation domains appear above and below the molecular plane at the carbon atoms. These domains become much more pronounced at delocalization radii of $d = 4.5$ and 6.0 au, respectively (post-vicinal delocalization; Figure 2i−l,m−p). In case of ethylene, where additional carbon−carbon interactions cannot occur beyond $d = 2.5$ au, both $\Gamma_X(4.5,\mathbf{r})$ and $\Gamma_X(6.0,\mathbf{r})$

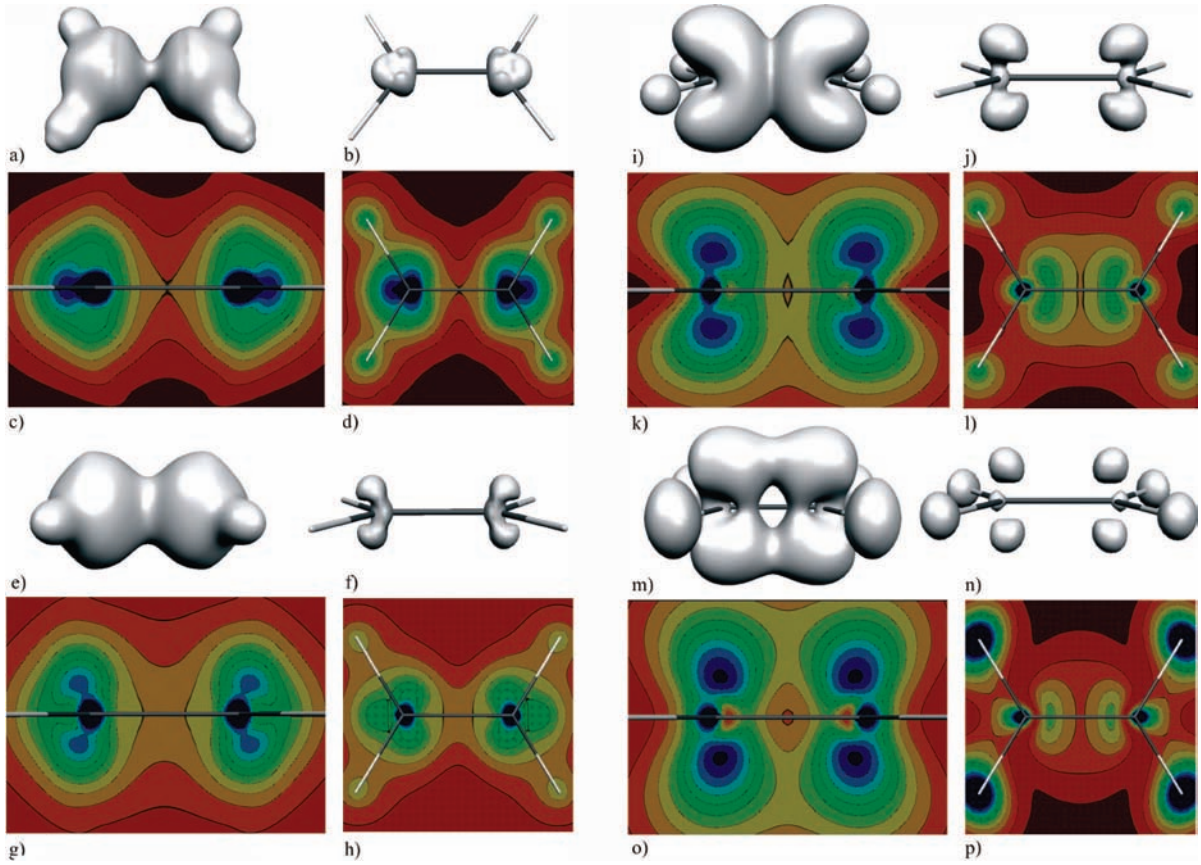

Figure 2. Same as Figure 1. (a) $\Gamma_X(2.5,\mathbf{r}) = -0.02$ au. (b) $\Gamma_X(2.5,\mathbf{r}) = -0.053$ au. (c,d) $\Gamma_X(2.5,\mathbf{r})$: starting value $= -0.01$ au, step size $= 0.006$ au. (e) $\Gamma_X(3.0,\mathbf{r}) = -0.01$ au. (f) $\Gamma_X(3.0,\mathbf{r}) = -0.035$. (g,h) $\Gamma_X(3.0,\mathbf{r})$: starting value $= -0.001$ au, step size $= 0.005$ au. (i) $\Gamma_X(4.5,\mathbf{r}) = -3.3 \times 10^{-3}$ au. (j) $\Gamma_X(4.5,\mathbf{r}) = -6.5 \times 10^{-3}$ au. (k,l) $\Gamma_X(4.5,\mathbf{r})$: starting value $= -0.001$ au, step size $= 8 \times 10^{-4}$ au. (m) $\Gamma_X(6.0,\mathbf{r}) = -5 \times 10^{-4}$ au. (n) $\Gamma_X(6.0,\mathbf{r}) = -0.001$ au. (o,p) $\Gamma_X(6.0,\mathbf{r})$: starting value $= -2 \times 10^{-4}$ au, step size $= 1 \times 10^{-4}$ au.

have very similar structures. The observed real space reflection of topological properties of π orbitals in the structure of $\Gamma_X(d,\mathbf{r})$ for $d \geq 3$ au is a remarkable feature, which is absent in the electron density or its Laplacian (the electron localization function provides a different view: a single dumbbell-shaped region perpendicular to the molecular plane, centered at the midpoint of the C−C bond).[6] This and the following examples point at the importance of π delocalization, if present, for distances which are larger than the mean spacing between two directly bonded carbon atoms.

The radial exchange density of acetylene **2** ($D_{\infty h}$; d(C−C) = 1.196 Å = 2.261 au) is shown in Figure 3 for $d = 1.5$ (3a−c), 2.5 (3d−f), 4.5 (3g−i) and 6.0 au (3j−l).

It is obvious that the four different radii are associated with the same general structure characteristics as in ethylene **1**. However, in this triply bonded molecule, the separated accumulation domains in $\Gamma_X(4.5,\mathbf{r})$ and $\Gamma_X(6.0,\mathbf{r})$ above and below the carbon atoms of ethylene are replaced by toroidal domains, which reflect the rotational symmetric delocalization implied by two perpendicular π molecular orbitals. Ethane **3** (D_{3d}; d(C−C) = 1.529 Å = 2.889 au), which is displayed in Figure 4, shows again similar relations between d range and general structure of $\Gamma_X(d,\mathbf{r})$, but $\Gamma_X(4.5,\mathbf{r})$ and $\Gamma_X(6.0,\mathbf{r})$ (Figure 4g−i,j−l) contain no π orbital density-like or torus-like features at the singly bonded carbon atoms.

$\Gamma_X(1.5,\mathbf{r})$ in ethane (Figure 4a−c) resembles $\nabla^2\rho(\mathbf{r})$ in number and position of its minima along the bonds, while in the case of acetylene **2** (Figure 3a−c) this analogy is less pronounced: $\Gamma_X(1.5,\mathbf{r})$ contains here two minima between the carbon centers, while $\nabla^2\rho(\mathbf{r})$ features only one.[6] Similarities between the negative value range of $\nabla^2\rho(\mathbf{r})$ and $\Gamma_X(d,\mathbf{r})$ at delocalization radii below bond distances are not unexpected, because minima in $\nabla^2\rho(\mathbf{r})$ are associated with regions of enhanced electron localization,[6–10] that is, regions where delocalization should occur predominantly over short distances.

Formal replacement of a carbon atom in ethylene **1** by the more electronegative and electron-rich nitrogen atom leads to methylenimine **4** ($H_2C{=}NH$, C_s; d(C−N) = 1.265 Å = 2.390 au). In all of the displayed d ranges (Figures 5 and 6c,d), $\Gamma_X(d,\mathbf{r})$ accumulates much stronger at the nitrogen atom than at carbon; that is, the basin with higher electron population ($\bar{N}$(N) = 8.251, $\bar{N}$(C) = 5.086) is here associated also with stronger delocalization (this must not necessarily be the case).

Analogous to ethylene **1**, $\Gamma_X(1.5,\mathbf{r})$ features regions of thinning above and below the molecular plane at the carbon and nitrogen atoms. Also like in **1**, the carbon core region is surrounded by three accumulation domains oriented along the bonds (Figure 5b,d), but the situation at nitrogen appears more complicated (Figure 5c,d). Noticeable is the presence of a separated domain in the region where the lone pair of the nitrogen atom is expected. In the same direction, $\Gamma_X(2.5,\mathbf{r})$ has at the nitrogen atom its largest spatial extension (Figure 5i). The shapes of the regions associated with delocalization over $d = 4.5$ au (Figure 5 k−o) are very similar to the ones in ethylene **1** and contain distinct π orbital density-like structures. $\Gamma_X(6.0,\mathbf{r})$ (Figure 5 p−t) appears somewhat different, because there occurs additional strong accumulation in the lone pair region. It is of interest, whether the radial exchange density resolves more than one lone pair domain per atom, if present. In the case of formaldehyde **5** ($H_2C{=}O$, C_{2v}; d(C−O) = 1.201 Å = 2.269

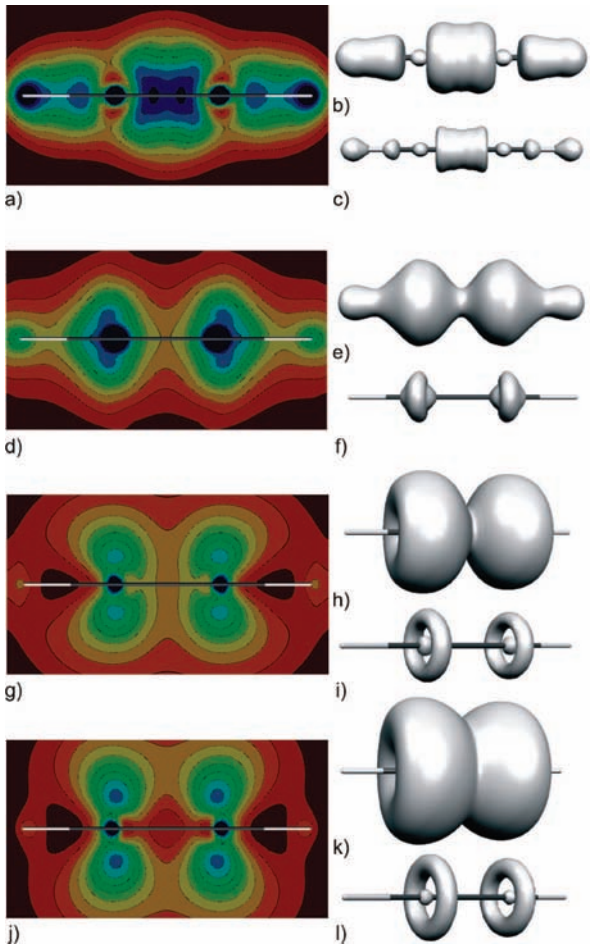

Figure 3. Radial exchange density in acetylene **2**. a,d,g,j: Contour line diagrams (cf. Figure 1) in the molecular plane. b,c,e,f,h,i,k,l: Isosurface representations. (a) $\Gamma_X(1.5,\mathbf{r})$: starting value = −0.03 au, step size = 0.015 au. (b) $\Gamma_X(1.5,\mathbf{r}) = -0.11$ au. (c) $\Gamma_X(1.5,\mathbf{r}) = -0.15$ au. (d) $\Gamma_X(2.5,\mathbf{r})$: starting value = −0.01 au, step size = 0.006 au. (e) $\Gamma_X(2.5,\mathbf{r}) = -0.025$ au. (f) $\Gamma_X(2.5,\mathbf{r}) = -0.055$ au. (g) $\Gamma_X(4.5,\mathbf{r})$: starting value = −0.001 au, step size = 8×10^{-4} au. (h) $\Gamma_X(4.5,\mathbf{r}) = -3.1 \times 10^{-3}$ au. (i) $\Gamma_X(4.5,\mathbf{r}) = -6.5 \times 10^{-3}$ au. j) $\Gamma_X(6.0,\mathbf{r})$: starting value = -2×10^{-4} au, step size = 8×10^{-5} au. (k) $\Gamma_X(6.0,\mathbf{r}) = -4 \times 10^{-4}$ au. (l) $\Gamma_X(6.0,\mathbf{r}) = -8 \times 10^{-4}$ au.

au), for which the Laplacian of the electron density indicates two lone pair domains at oxygen, it turns out that these are clearly visible in $\Gamma_X(1.0,\mathbf{r})$ (Figure 6a,b), while only a single domain is present at d = 1.5 and 2.5 au (at 4.5 and 6.0 au, there appear again two separate domains).

A delocalization radius of 1.0 au is also better suited to resolve the lone pair domain in methylenimine **4** (Figure 6c,d). In both cases, the domains indicated by $\Gamma_X(1.0,\mathbf{r})$ are located very close to these in $\nabla^2\rho(\mathbf{r})$. Regarding **4**, it should further be noted, that the structure of $\Gamma_X(1.0,\mathbf{r})$ at nitrogen corresponds approximately to the structure of $\Gamma_X(1.5,\mathbf{r})$ at carbon (Figure 5 a−e).

The examples given so far provide an impression of basic properties of $\Gamma_X(d,\mathbf{r})$ in small molecules. In the following, some effects of bond conjugation on $\Gamma_X(d,\mathbf{r})$ will be examined. Trans-1,3-butadiene **6** ($H_2C^1{=}C^2H_2{-}C^3H_2{=}C^4H_2$, C_{2h}; d(C1−C2) = 1.335 Å = 2.523 au, d(C2−C3) = 1.454 Å = 2.748 au) is the prototype of conjugated polyenes. It is of interest, here, that the total π delocalization between C1 and C3 is less pronounced than that between C1 and C4 (cf. also octatetraene[26,73] and $C_{24}H_{26}$[108]): the delocalization indices evaluated by using only π molecular orbitals[109] in eq 4 amount to δ^π(C1,C2) = 0.796, δ^π(C1,C3) = 0.037, δ^π(C1,C4) = 0.072 and δ^π(C2,C3) = 0.140.

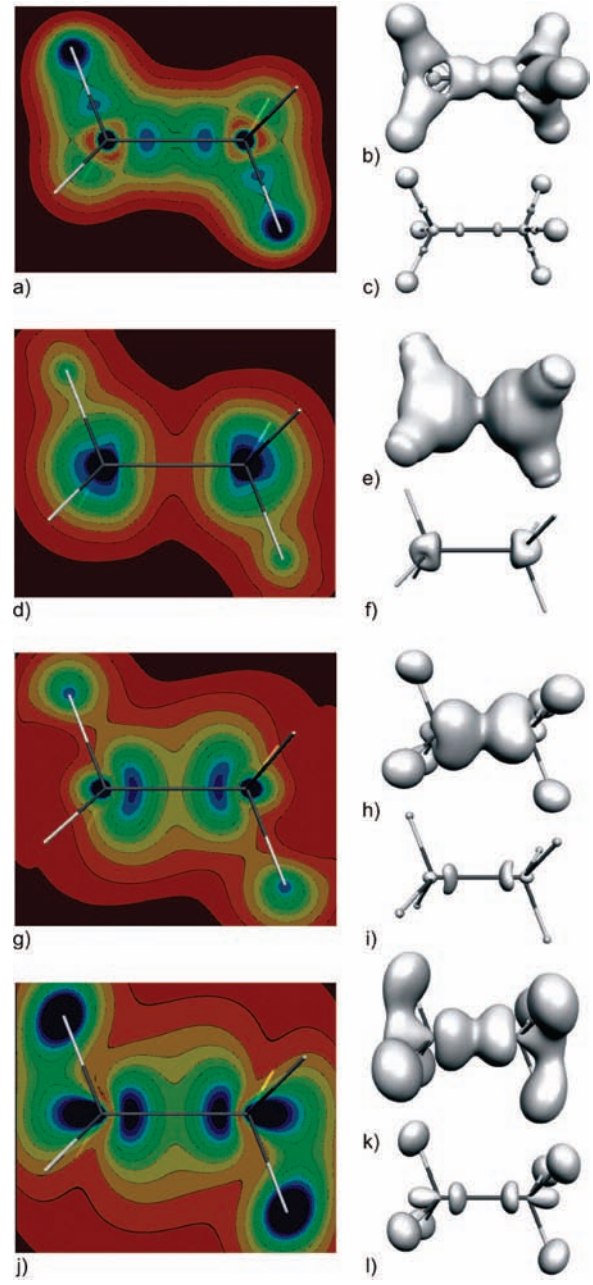

Figure 4. Radial exchange density in ethane **3**. a,d,g,j: Contour line diagrams (cf. Figure 1) in planes containing two carbon and two hydrogen atoms. b,c,e,f,h,i,k,l: Isosurface representations. (a) $\Gamma_X(1.5,\mathbf{r})$: starting value = −0.03 au, step size = 0.015 au. (b) $\Gamma_X(1.5,\mathbf{r}) = -0.11$ au. (c) $\Gamma_X(1.5,\mathbf{r}) = -0.15$ au. (d) $\Gamma_X(2.5,\mathbf{r})$: starting value = −0.01 au, step size = 0.006 au. (e) $\Gamma_X(2.5,\mathbf{r}) = -0.017$ au. (f) $\Gamma_X(2.5,\mathbf{r}) = -0.055$ au. (g) $\Gamma_X(4.5,\mathbf{r})$: starting value = −0.001 au, step size = 7×10^{-4} au. (h) $\Gamma_X(4.5,\mathbf{r}) = -3.3 \times 10^{-3}$ au. (i) $\Gamma_X(4.5,\mathbf{r}) = -6.5 \times 10^{-3}$ au. (j) $\Gamma_X(6.0,\mathbf{r})$: starting value = -1×10^{-4} au, step size = 1×10^{-4} au. (k) $\Gamma_X(6.0,\mathbf{r}) = -5 \times 10^{-4}$ au. (l) $\Gamma_X(6.0,\mathbf{r}) = -9 \times 10^{-4}$ au.

Because there are additional σ contributions to 1,3-delocalization, these differences are smaller, but still recognizable, in the total delocalization indices: δ(C1,C2) = 1.791, δ(C1,C3) = 0.074, δ(C1,C4) = 0.077 and δ(C2,C3) = 1.091. Consideration of the qualitatively most probable[110] ionic resonance structures[44,49,50,115] for the π electrons likewise predicts negative correlations[116] in the pair density,[49,51,52] that is, delocalization, to occur mainly between C1 and C2 (II, III) or C1 and C4 (III, IV), respectively:

Both $\Gamma_X(1.5,\mathbf{r})$ and $\Gamma_X(2.5,\mathbf{r})$ (Figure 7a,b and c,d) are essentially unchanged with respect to ethylene **1**, what is at least

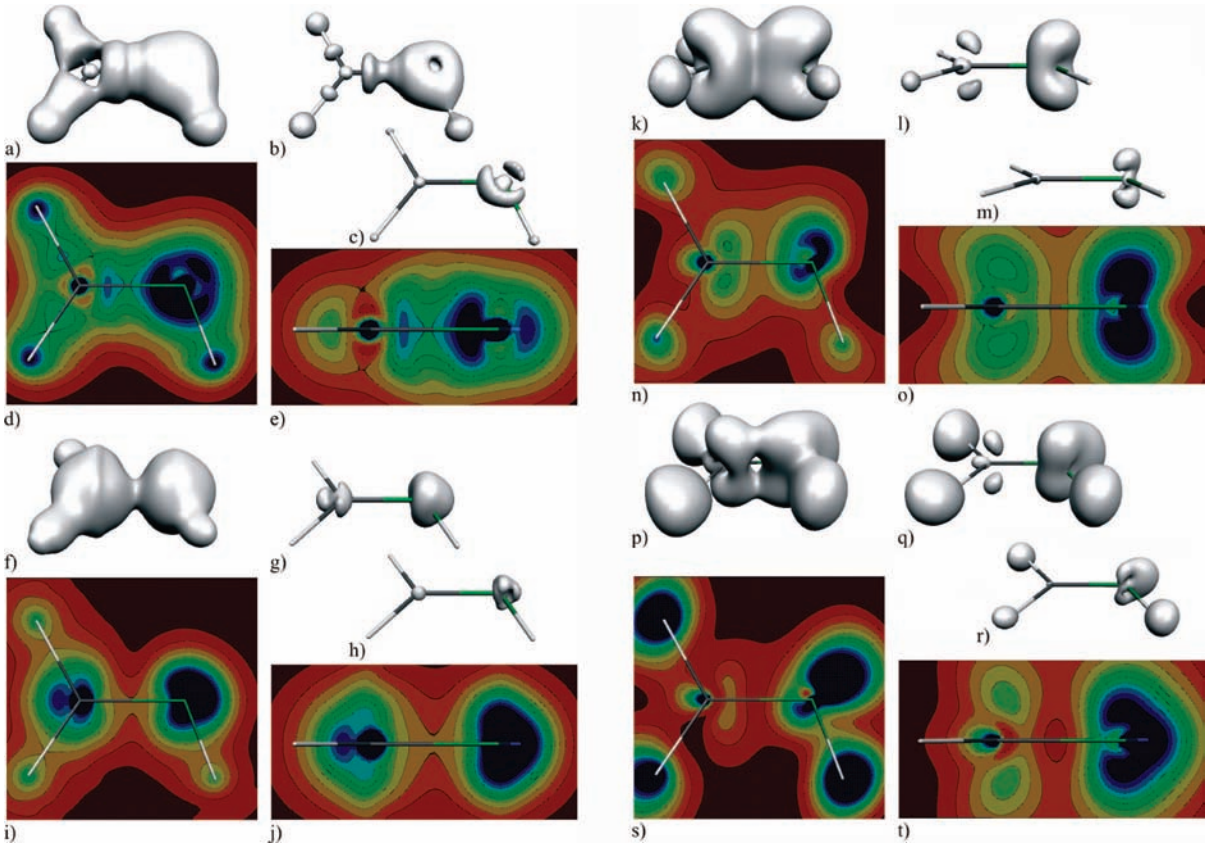

Figure 5. Radial exchange density in methylenimine **4**. a,b,c,f,g,h,k,l,m,p,q,r: Isosurface representations. d,e,i,j,n,o,s,t: Contour line diagrams (cf. Figure 1) in planes containing the carbon and nitrogen nuclei, parallel (d,i,n,s) and perpendicular (e,j,o,t) to the molecular plane. (a) $\Gamma_X(1.5,\mathbf{r}) = -0.11$ au. (b) $\Gamma_X(1.5,\mathbf{r}) = -0.15$ au. (c) $\Gamma_X(1.5,\mathbf{r}) = -0.22$ au (d,e) $\Gamma_X(1.5,\mathbf{r})$: starting value $= -0.02$ au, step size $= 0.02$ au. (f) $\Gamma_X(2.5,\mathbf{r}) = -0.02$ au. (g) $\Gamma_X(2.5,\mathbf{r}) = -0.058$ au. (h) $\Gamma_X(2.5,\mathbf{r}) = -0.09$ au. (i,j) $\Gamma_X(2.5,\mathbf{r})$: starting value $= -0.01$ au, step size $= 0.006$ au. (k) $\Gamma_X(4.5,\mathbf{r}) = -2.6 \times 10^{-3}$ au. (l) $\Gamma_X(4.5,\mathbf{r}) = -0.005$ au. (m) $\Gamma_X(4.5,\mathbf{r}) = -8.5 \times 10^{-3}$ au. (n,o) $\Gamma_X(4.5,\mathbf{r})$: starting value $= -0.001$ au, step size $= 7 \times 10^{-4}$ au. (p) $\Gamma_X(6.0,\mathbf{r}) = -3 \times 10^{-4}$ au. (q) $\Gamma_X(6.0,\mathbf{r}) = -5 \times 10^{-4}$ au. (r) $\Gamma_X(6.0,\mathbf{r}) = -0.001$ au. (s,t) $\Gamma_X(6.0,\mathbf{r})$: starting value $= -2 \times 10^{-4}$ au, step size $= 8 \times 10^{-5}$ au.

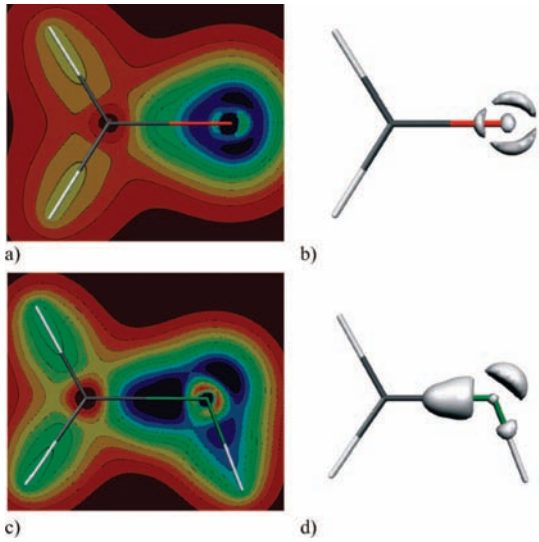

Figure 6. Radial exchange density in formaldehyde **5** (a,b) and methylenimine **4** (c,d). a,c: Contour line diagrams (cf. Figure 1) in the molecular planes. b,d: Isosurface representations. (a) $\Gamma_X(1.0,\mathbf{r})$: starting value $= -0.02$ au, step size $= 0.06$ au. (b) $\Gamma_X(1.0,\mathbf{r}) = -0.6$ au. (c) $\Gamma_X(1.0,\mathbf{r})$: starting value $= -0.03$ au, step size $= 0.03$ au. (d) $\Gamma_X(1.0,\mathbf{r}) = -0.31$ au.

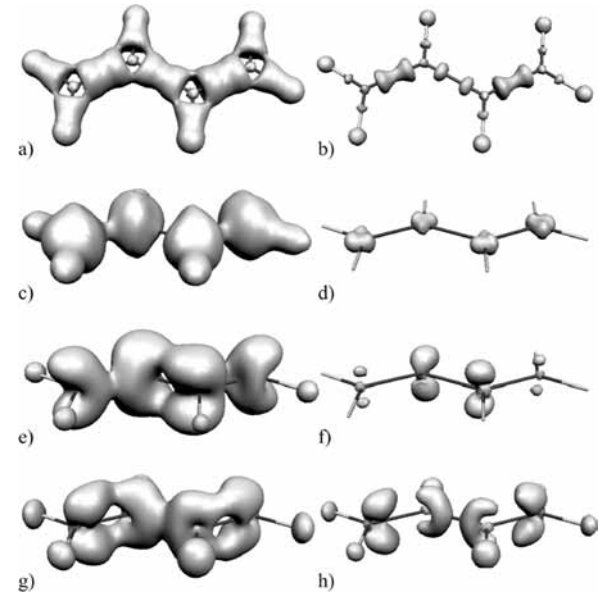

Figure 7. Radial exchange density in butadiene **6**. Isosurface representations. (a) $\Gamma_X(1.5,\mathbf{r}) = -0.11$ au. (b) $\Gamma_X(1.5,\mathbf{r}) = -0.15$ au. (c) $\Gamma_X(2.5,\mathbf{r}) = -0.02$ au. (d) $\Gamma_X(2.5,\mathbf{r}) = -0.053$ au. (e) $\Gamma_X(4.5,\mathbf{r}) = -3.3 \times 10^{-3}$ au. (f) $\Gamma_X(4.5,\mathbf{r}) = -6.5 \times 10^{-3}$ au. (g) $\Gamma_X(6.0,\mathbf{r}) = -8 \times 10^{-4}$ au. (h) $\Gamma_X(6.0,\mathbf{r}) = -1.1 \times 10^{-3}$ au.

for $\Gamma_X(1.5,\mathbf{r})$ understandable, as it measures delocalization over a distance, which is significantly below the range of C−C bond lengths.

The 1,3-carbon−carbon distance (d(C1−C3) = d(C2−C4)) in **6** amounts to 4.662 au (2.467 Å); hence, $\Gamma_X(4.5,\mathbf{r})$ (Figure 7e,f) at the carbon atoms includes significant fractions of 1,3-

SCHEME 1: Resonance structures for butadiene 6

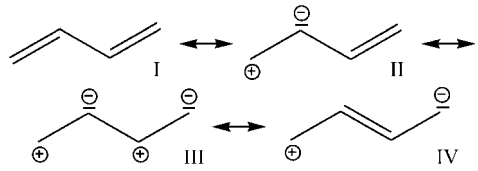

C/C delocalization (C1/C3 and C2/C4). Similar to the case of ethylene **1**, $\Gamma_X(4.5,\mathbf{r})$ contains characteristic π orbital density-like structure elements at the carbon atoms. However, it is not a simple union of the corresponding functions for two ethylene molecules; it accumulates more strongly at the central carbon atoms than at the terminal ones, although the atomic electron populations are almost identical ($\bar{N}(C1) = \bar{N}(C4) = 5.986$, $\bar{N}(C2) = \bar{N}(C3) = 5.983$). To some extent, this is due to the fact that large parts of the integration sphere surface are located rather distant from any atomic center, when **r** is at the terminal carbon atom. Upon raising the delocalization radius to $d = 6.0$ au (3.175 Å), these differences decrease (Figure 7g,h); the sphere surfaces for **r** at the central carbon atoms are then outside both carbon chain termini, while the sphere surfaces for **r** at the terminal atoms approach the basins of the opposite terminal carbon atoms (d(C1−C4) = 3.691 Å = 6.975 au), to which π delocalization is stronger than in the preceding case of 1,3-delocalization at $d = 4.5$ au. The isosurface for $\Gamma_X(6.0,\mathbf{r}) = -8 \times 10^{-4}$ au (Figure 7g) appears in conceptual conformance to the Lewis formula representation of butadiene, as being composed of two terminal double and a central single carbon−carbon bond, but this is not a general result, what will become evident in the discussion of vinylacetylene **8**.

In butatriene **7** ($H_2C^1{=}C^2{=}C^3{=}C^4H_2$, D_{2h}; d(C1−C2) = 1.313 Å = 2.481 au, d(C2−C3) = 1.264 Å = 2.389 au), the central single bond of **6** is replaced by an additional double bond, whose constituting p_π atomic orbitals are oriented perpendicular to those of the terminal double bonds. The regions associated with proximal delocalization at $d = 1.5$ au (Figure 8a,b) resemble ethylene **1** at the terminal and acetylene **2** at the central carbon atoms, respectively, while at $d = 2.5$ au (Figure 8c,d) no pronounced differences to butadiene **6** are discernible.

In $\Gamma_X(4.5,\mathbf{r})$ (Figure 8e,f) occur π orbital density-like structures at the terminal carbon atoms, while the central ones

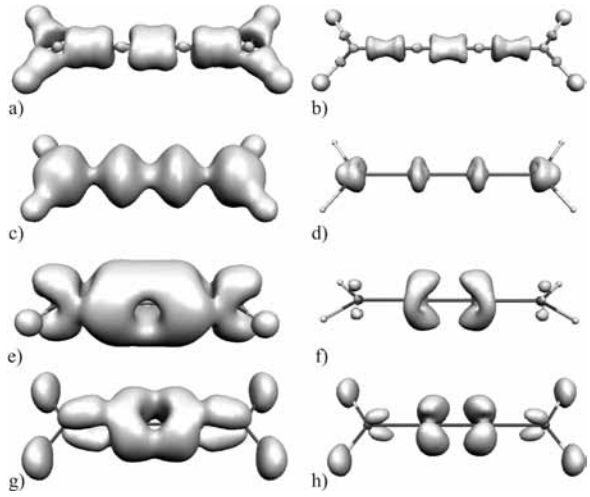

Figure 8. Radial exchange density in butatriene **7**. Isosurface representations. (a) $\Gamma_X(1.5,\mathbf{r}) = -0.11$ au. (b) $\Gamma_X(1.5,\mathbf{r}) = -0.15$ au. (c) $\Gamma_X(2.5,\mathbf{r}) = -0.022$ au. (d) $\Gamma_X(2.5,\mathbf{r}) = -0.05$ au. (e) $\Gamma_X(4.5,\mathbf{r}) = -2.6 \times 10^{-3}$ au. (f) $\Gamma_X(4.5,\mathbf{r}) = -5.5 \times 10^{-3}$ au. (g) $\Gamma_X(6.0,\mathbf{r}) = -8 \times 10^{-4}$ au. (h) $\Gamma_X(6.0,\mathbf{r}) = -1.2 \times 10^{-3}$ au.

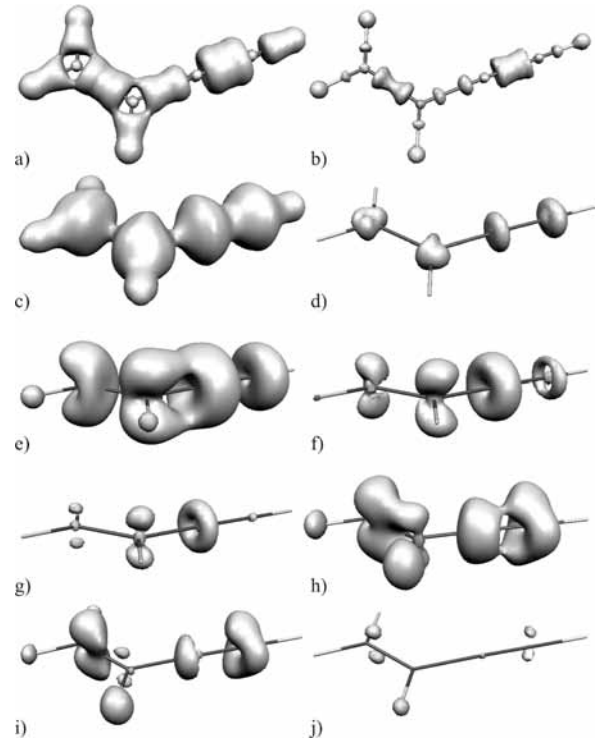

Figure 9. Radial exchange density in vinylacetylene **8**. Isosurface representations. (a) $\Gamma_X(1.5,\mathbf{r}) = -0.11$ au. (b) $\Gamma_X(1.5,\mathbf{r}) = -0.15$ au. (c) $\Gamma_X(2.5,\mathbf{r}) = -0.02$ au. (d) $\Gamma_X(2.5,\mathbf{r}) = -0.05$ au. (e) $\Gamma_X(4.5,\mathbf{r}) = -3.3 \times 10^{-3}$ au. (f) $\Gamma_X(4.5,\mathbf{r}) = -5 \times 10^{-3}$ au. (g) $\Gamma_X(4.5,\mathbf{r}) = -6.5 \times 10^{-3}$ au. (h) $\Gamma_X(6.0,\mathbf{r}) = -8 \times 10^{-4}$ au. (i) $\Gamma_X(6.0,\mathbf{r}) = -1.1 \times 10^{-3}$ au. (j) $\Gamma_X(6.0,\mathbf{r}) = -2.2 \times 10^{-3}$ au.

are surrounded by distorted toroidal domains, in which the out-of-plane π component dominates. As in the case of butadiene **7**, the total accumulation is stronger at the central than at the terminal carbon atoms. The expected perpendicular π orbital density-like structures appear more clearly at $d = 6.0$ au (Figure 8g,h), where the in-plane π component dominates over the out-of-plane component at the central carbon atoms (in contrast to **7**, the central accumulations remain distinctly stronger than the terminal ones). Again, the structure of $\Gamma_X(6.0,\mathbf{r})$ appears in conformance with the usual Lewis formula representation, that contains three adjacent carbon−carbon double bonds.

Vinylacetylene **8** ($HC^1{\equiv}C^2{-}C^3H{=}C^4H_2$, C_s; d(C1−C2) = 1.203 Å = 2.273 au, d(C2−C3) = 1.423 Å = 2.688 au, d(C3−C4) = 1.335 Å = 2.523 au) raises the question whether double and triple bonds retain their characteristic shapes in $\Gamma_X(4.5,\mathbf{r})$ and $\Gamma_X(6.0,\mathbf{r})$, that is, those observed in the basic units ethylene **1** and acetylene **2,** upon mutual conjugation. In the case of short delocalization radii, there is no qualitatively discernible interaction: $\Gamma_X(1.5,\mathbf{r})$ and $\Gamma_X(2.5,\mathbf{r})$ resemble closely the underlying building blocks **1** and **2** (Figure 9a,b and c,d).

In analogy to butadiene **6**, qualitative consideration of resonance structures suggest predominantly 1,2- and 1,4-delocalization to be present in the π system perpendicular to the molecular plain of **8**, what is line with the π delocalization indices:[117] $\delta^\pi(C1,C2) = 0.874$, $\delta^\pi(C1,C3) = 0.023$, $\delta^\pi(C1,C4) = 0.063$, $\delta^\pi(C2,C3) = 0.143$, $\delta^\pi(C2,C4) = 0.049$ and $\delta^\pi(C3,C4) = 0.799$. Hence, those π interactions between the double and the triple bond which are expected to be visible in $\Gamma_X(d,\mathbf{r})$, that is, which occur over distances larger than C−C bond lengths, should concern more 1,4- rather than 1,3-delocalization. The presence of the triple bond makes it impossible to infer this π resonance pattern from the total ($\sigma + \pi$) delocalization indices;

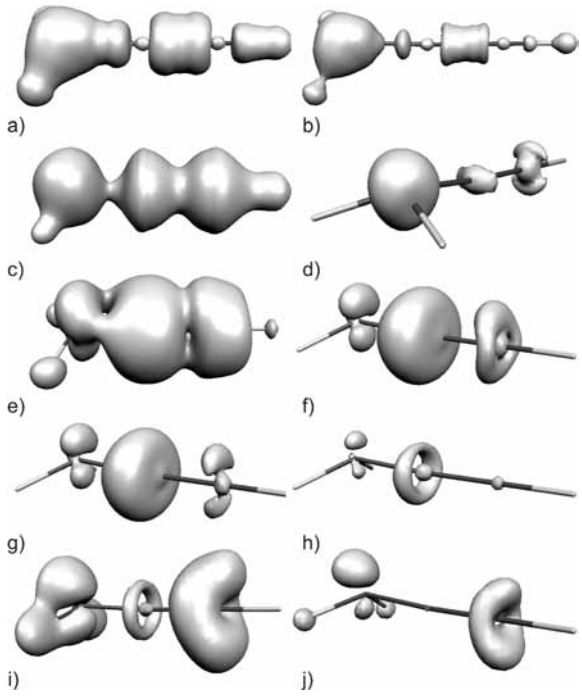

Figure 10. Radial exchange density in aminoacetylene **9**. Isosurface representations. (a) $\Gamma_X(1.5,\mathbf{r}) = -0.11$ au. (b) $\Gamma_X(1.5,\mathbf{r}) = -0.15$ au. (c) $\Gamma_X(2.5,\mathbf{r}) = -0.02$ au. (d) $\Gamma_X(2.5,\mathbf{r}) = -0.061$ au. (e) $\Gamma_X(4.5,\mathbf{r}) = -2.2 \times 10^{-3}$ au. (f) $\Gamma_X(4.5,\mathbf{r}) = -4.5 \times 10^{-3}$ au. (g) $\Gamma_X(4.5,\mathbf{r}) = -5 \times 10^{-3}$ au. (h) $\Gamma_X(4.5,\mathbf{r}) = -7.2 \times 10^{-3}$ au. (i) $\Gamma_X(6.0,\mathbf{r}) = -9 \times 10^{-4}$ au. (j) $\Gamma_X(6.0,\mathbf{r}) = -2 \times 10^{-3}$ au.

for the terminal olefin carbon atom (but not for the terminal acetylene carbon atom), 1,3-delocalization is larger than 1,4-delocalization: δ(C1,C2) = 2.662, δ(C1,C3) = 0.065, δ(C1,C4) = 0.075, δ(C2,C3) = 1.127, δ(C2,C4) = 0.095 and δ(C3,C4) = 1.787. Because the 1,3-carbon−carbon distances (d(C1−C3) and d(C2−C4)) in **8** amount to 4.960 au (2.625 Å) and 4.612 au (2.441 Å), respectively, $\Gamma_X(4.5,\mathbf{r})$ measures mainly 1,3-C/C delocalization. It contains simultaneously π orbital density-like and torus-shaped structures at the carbon atoms (Figure 9 e−g), which are similar to those in ethylene **1** and acetylene **2**. Like in **6** and **7**, $\Gamma_X(4.5,\mathbf{r})$ accumulates more pronounced at the central carbon atoms. The situation is different at $d = 6.0$ au (Figure 9 h−j), which includes 1,4-C/C delocalization; d(C1−C4) amounts to 6.742 au (3.568 Å), hence the basin of C4 can already be reached by the integration sphere surface for **r** within the basin of C1. In $\Gamma_X(6.0,\mathbf{r})$, the toroidal domain at the terminal triple bond carbon atom C1 is distorted towards the dumbbell-like structure of a p_π orbital, a shape which is transmitted from the terminal carbon atom C4 of the double bond, because conjugation can occur only within parallel π orbitals (cf. Figure 9f vs Figure 9j). In case of **6** and **7**, on the other hand, 1,4-delocalization has no distorting effects, because the conjugated bonds are of identical types.

In conjugated systems with an uneven number of participating atoms, where qualitative resonance structures indicate 1,3-delocalization to be important, the effects of conjugation on the shape of triple bond domains may already be apparent in the structure of $\Gamma_X(4.5,\mathbf{r})$. Aminoacetylene **9** ($H_2N^1-C^2\equiv C^3H$, C_s; d(N−C) = 1.352 Å = 2.555 au, d(C−C) = 1.201 Å = 2.269 au) is an example for such a system (δ(N1,C2) = 1.123, δ(C2,C3) = 2.570, δ(N1,C3) = 0.158):

The structure of $\Gamma_X(1.5,\mathbf{r})$ (Figure 10a,b) at the carbon atoms of **9** is approximately rotational symmetric, resembling strongly acetylene **2**, but in $\Gamma_X(2.5,\mathbf{r})$ (Figure 10c,d), the influence of the amino group on the acetylene unit is already obvious: at the terminal carbon atom, there is distinctly stronger accumulation parallel to the direction of the nitrogen lone pair region than perpendicular to it.

SCHEME 2: Resonance structures for aminoacetylene 9

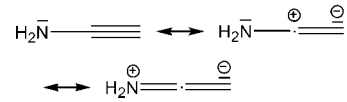

SCHEME 3: Homotropylium cation 10

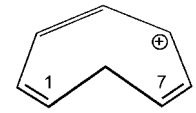

At a delocalization radius of 4.5 au (Figure 10 e−h), which is dominated by delocalization between nitrogen and the terminal carbon atom (d(N1−C3) = 2.552 Å = 4.823 au), the structural differences between both carbon atoms are very pronounced. $\Gamma_X(4.5,\mathbf{r})$ features a toroidal domain at the central carbon atom (Figure 10h), but at the terminal one, this domain is strongly distorted, appearing with distinct π orbital density-like structure elements at an isosurface value of -5×10^{-3} au (Figure 10g). Obviously, this imprint of the similar shaped region at the nitrogen atom into the terminal triple bond torus is in line with the expected pattern of resonance structures (Scheme 2). Raising the delocalization radius to 6.0 au (Figure 10i,j) causes no significant qualitative alterations, but in analogy to molecules **6** and **8**, the degree of accumulation increases at the outer atoms, while it decreases at the inner one.

In some special cases of nonplanar molecules, conjugation of functional groups is assumed to occur directly through space instead of through intermediate bonds (homoconjugation). A classic example is the homotropylium cation **10** ($C_8H_9^+$, C_s),[118] which is regarded on the basis of structural and magnetic criteria as a cyclically conjugated 6π electron system, with homoconjugation of the multiple bonds occuring across the space between the methylene-bridged carbon atoms C1 and C7 (d(C1−C7) = 2.148 Å = 4.059 au):

Although there is no bond path present between these two atoms, the delocalization index δ(C1,C7) is with 0.240 rather high for a pair of nonbonded atoms. The presence of direct delocalization between C1 and C7 is reflected in the shapes of atomic exchange densities (DAFH's) and their Laplacians.[119] It is therefore of interest whether the radial exchange density likewise contains indications for homoconjugation. The structures of $\Gamma_X(d,\mathbf{r})$ at $d = 1.5$ and 2.5 au (Figure 11a,b and c,d) exhibit no special features and are in line with those of ethylene **1** and butadiene **6**.

Of particular interest, on the other hand, are $\Gamma_X(4.5,\mathbf{r})$ and $\Gamma_X(6.0,\mathbf{r})$ (Figure 11e,f and g,h), which contain π orbital density-like structures at all trigonal coordinated carbon atoms. At low absolute isosurface values (Figure 11e and g), these structures melt together at adjacent atoms, so that C1 and C7 become directly linked through a separated zone below the methylene group, a situation which resembles the familiar description of homoconjugation by means of obliquely overlapping p_π atomic orbitals.

Conclusions

It has been shown that angular integration of the exchange density is a useful method for the partial visualization of its six-dimensional structure in three-dimensional space. Besides

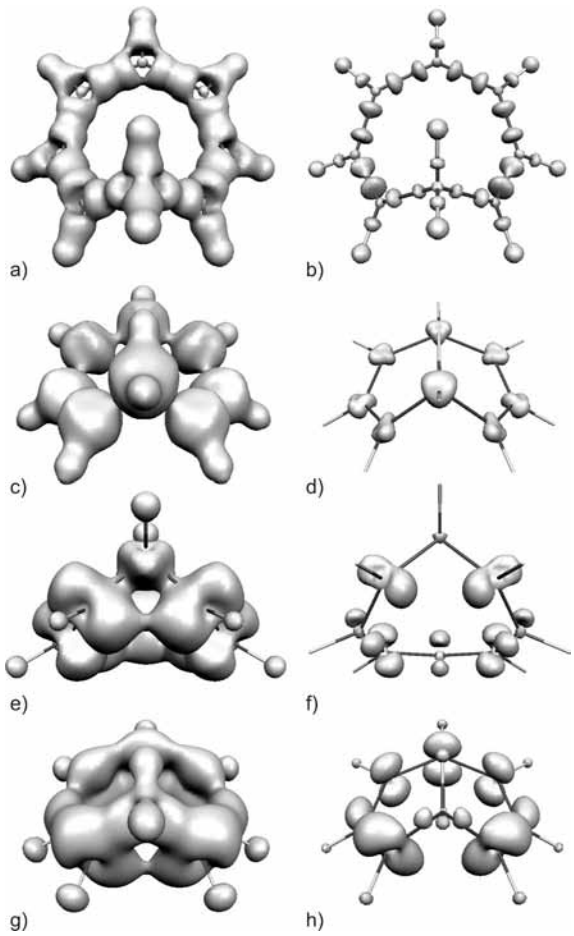

Figure 11. Radial exchange density in the homotropylium cation **10**. Isosurface representations. (a) $\Gamma_X(1.5,\mathbf{r}) = -0.11$ au. (b) $\Gamma_X(1.5,\mathbf{r}) = -0.15$ au. (c) $\Gamma_X(2.5,\mathbf{r}) = -0.02$ au. (d) $\Gamma_X(2.5,\mathbf{r}) = -0.05$ au. (e) $\Gamma_X(4.5,\mathbf{r}) = -3.3 \times 10^{-3}$ au. (f) $\Gamma_X(4.5,\mathbf{r}) = -6.5 \times 10^{-3}$ au. (g) $\Gamma_X(6.0,\mathbf{r}) = -1 \times 10^{-3}$ au. (h) $\Gamma_X(6.0,\mathbf{r}) = -2 \times 10^{-3}$ au.

its clear physical meaning as a measure of correlations in the pair density (which equals electron delocalization at the HF level), an important aspect of the exchange density (or the related Fermi hole) is that its structure, despite being invariant with respect to unitary orbital transformations, reflects some of the familiar aspects of orbital shapes.[10,23,66,73] This property, which is known from representations for fixed reference points or basins, survives angular integration. In the context of completely orbital-independent descriptions of electronic structures, the extraction of invariant shape aspects of orbital models from wavefunctions is expected to become increasingly important in the future. It should be noted that the analysis described in this work is not limited to the Hartree−Fock level; besides substituting $\Gamma_X(\mathbf{r}_1,\mathbf{r}_2)$ with the general exchange-correlation density, it is also of interest to employ the sharing index instead.

On the whole, the structure of $\Gamma_X(d,\mathbf{r})$ in carbon multiple bond systems fits to the picture of a local σ type scaffolding, which is overlaid by long-range π delocalization. Small delocalization radii are associated mainly with atomic core regions ($d = 0.5$ au), while somewhat farther reaching delocalization ($d = 1.0$ and 1.5 au) originates from regions, which resemble characteristic structure elements of $\nabla^2\rho(\mathbf{r})$, like its bonded and nonbonded (lone pair) minima in the valence shell charge concentration. Because both σ and π delocalization are involved in C−C multiple bonds, the radial exchange density resolves no π contributions at radii in the range of the corresponding bond distances ($d = 2.5$ au). On the other hand, radii corresponding to 1,3-delocalization ($d = 4.5$ au) or above ($d = 6.0$ au) are associated mainly with π orbital density-similar structures, because of the increasing importance of π delocalization for non-nearest neighbor interactions.

Supporting Information Available: Cartesian coordinates (in atomic units) of **1** – **10**. This material is available free of charge via the Internet at http://pubs.acs.org.

References and Notes

(1) Löwdin, P.-O. *Phys. Rev.* **1955**, *97*, 1474.
(2) McWeeny, R. *Rev. Mod. Phys.* **1960**, *32*, 335.
(3) Bader, R. F. W. *Chem. Rev.* **1991**, *91*, 893.
(4) Bader, R. F. W. *J. Phys. Chem. A* **2007**, *111*, 7966.
(5) Bader, R. F. W. *Atoms in Molecules - A Quantum Theory*; Oxford University Press: Oxford, U.K., 1990.
(6) Bader, R. F. W.; Johnson, S.; Tang, T.-H.; Popelier, P. L. A. *J. Phys. Chem.* **1996**, *100*, 15398.
(7) Bader, R. F. W.; Heard, G. L. *J. Chem. Phys.* **1999**, *111*, 8789.
(8) Malcolm, N. O. J.; Popelier, P. L. A. *Faraday Discuss.* **2003**, 124.
(9) Popelier, P. L. A. *Coord. Chem. Rev.* **2000**, *197*, 169.
(10) Bader, R. F. W.; Gillespie, R. J.; MacDougall, P. J. *J. Am. Chem. Soc.* **1988**, *110*, 7329.
(11) Becke, A. D.; Edgecombe, K. E. *J. Chem. Phys.* **1990**, *92*, 5397.
(12) Silvi, B. *J. Phys. Chem. A* **2003**, *107*, 3081.
(13) Savin, A.; Nesper, R.; Wengert, S.; Fässler, T. *Angew. Chem. Int. Ed. Engl.* **1997**, *36*, 1808.
(14) Matito, E.; Silvi, B.; Duran, M.; Solà, M. *J. Chem. Phys.* **2006**, *125*, 024301.
(15) Kohout, M. *Int. J. Quant. Chem.* **2004**, *97*, 651.
(16) Kohout, M.; Pernal, K.; Wagner, F. R.; Grin, Y. *Theor. Chem. Acc.* **2004**, *112*, 453.
(17) Kohout, M. *Faraday Discuss.* **2007**, *135*, 43.
(18) Schmider, H. L.; Becke, A. D. *J. Chem. Phys.* **2002**, *116*, 3184.
(19) Scemama, A.; Caffarel, M.; Savin, A. *J. Comput. Chem.* **2007**, *28*, 442.
(20) Bader, R. F. W.; Streitwieser, A.; Neuhaus, A.; Laidig, K. E.; Speers, P. *J. Am. Chem. Soc.* **1996**, *118*, 4959.
(21) Ruedenberg, K. *Rev. Mod. Phys.* **1962**, *34*, 326.
(22) Fradera, X.; Poater, J.; Simon, S.; Duran, M.; Solà, M. *Theor. Chem. Acc.* **2002**, *108*, 214.
(23) Buijse, M. A.; Baerends, E. J. *Mol. Phys.* **2002**, *100*, 401.
(24) Fulton, R. L. *J. Phys. Chem.* **1993**, *97*, 7516.
(25) Fulton, R. L. *J. Phys. Chem. A* **2006**, *110*, 12191.
(26) Gill, P. M. W.; Lee, A. M.; Nair, N.; Adamson, R. D. *J. Mol. Struct. (Theochem)* **2000**, *506*, 303.
(27) Lee, A. M.; Gill, P. M. W. *Chem. Phys. Lett.* **1999**, *313*, 271.
(28) Fradera, X.; Duran, M.; Mestres, J. *J. Chem. Phys.* **2000**, *113*, 2530.
(29) Lennard-Jones, J. E. *J. Chem. Phys.* **1952**, *20*, 1024.
(30) Fradera, X.; Austen, M. A.; Bader, R. F. W. *J. Phys. Chem. A* **1999**, *103*, 304.
(31) Bader, R. F. W.; Stephens, M. E. *J. Am. Chem. Soc.* **1975**, *97*, 7391.
(32) Poater, J.; Solà, M.; Duran, M.; Fradera, X. *Theor. Chem. Acc.* **2002**, *107*, 362.
(33) Fradera, X.; Solà, M. *J. Comput. Chem.* **2002**, *23*, 1347.
(34) Matito, E.; Solà, M.; Salvador, P.; Duran, M. *Faraday Discuss.* **2007**, *135*, 325.
(35) Rincón, L.; Alvarellos, J. E.; Almeida, R. *J. Chem. Phys.* **2005**, *122*, 214103.
(36) Wang, Y.-G.; Werstiuk, N. H. *J. Comput. Chem.* **2003**, *24*, 379.
(37) Wang, Y.-G.; Matta, C.; Werstiuk, N. H. *J. Comput. Chem.* **2003**, *24*, 1720.
(38) Wang, Y.-G.; Wiberg, K. B.; Werstiuk, N. H. *J. Phys. Chem. A* **2007**, *111*, 3592.
(39) Chesnut, D. B. *Chem. Phys.* **2006**, *327*, 327.
(40) Ponec, R.; Cooper, D. L. *J. Mol. Struct. (Theochem)* **2005**, *727*, 133.
(41) Ponec, R.; Cooper, D. L. *J. Phys. Chem. A* **2007**, *111*, 11294.
(42) Bader, R. F. W.; Stephens, M. E. *Chem. Phys. Lett.* **1974**, *26*, 445.
(43) Silvi, B. *Phys. Chem. Chem. Phys.* **2004**, *6*, 256.
(44) Schütt, J.; Böhm, M. C. *J. Am. Chem. Soc.* **1992**, *114*, 7252.
(45) Böhm, M. C.; Schmitt, U.; Schütt, J. *J. Phys. Chem.* **1993**, *97*, 11427.
(46) Böhm, M. C.; Schütt, J.; Philipp, S. *Int. J. Quant. Chem.* **1998**, *69*, 727.

(47) Francisco, E.; Martín Pendás, A.; Blanco, M. A. *J. Chem. Phys* **2007**, *126*, 094102.
(48) Francisco, E.; Martín Pendás, A.; Blanco, M. A. *J. Chem. Phys* **2007**, *127*, 144103.
(49) Martín Pendás, A.; Francisco, E.; Blanco, M. A. *Phys. Chem. Chem. Phys* **2007**, *9*, 1087.
(50) Parrondo, R. M.; Karafiloglou, P.; Sánchez Marcos, E. *Int. J. Quant. Chem* **1994**, *52*, 1127.
(51) Karafiloglou, P. *J. Phys. Chem. A* **2001**, *105*, 4524.
(52) Karafiloglou, P.; Launay, J.-P. *Chem. Phys.* **2003**, *289*, 231.
(53) Karafiloglou, P. *Chem. Phys.* **1990**, *140*, 373.
(54) Martín Pendás, A.; Francisco, E.; Blanco, M. A. *J. Phys. Chem. A* **2006**, *110*, 12864.
(55) Baerends, E. J.; Gritsenko, O. V. *J. Phys. Chem. A* **1997**, *101*, 5383.
(56) Kar, T.; Ángyán, J. G.; Sannigrahi, A. B. *J. Phys. Chem. A* **2000**, *104*, 9953.
(57) Luken, W. L. *Int. J. Quant. Chem.* **1982**, *22*, 889.
(58) Ángyán, J. G.; Loos, M.; Mayer, I. *J. Phys. Chem.* **1994**, *98*, 5244.
(59) Bochicchio, R. C.; Lain, L.; Torre, A. *Chem. Phys. Lett.* **2003**, *374*, 567.
(60) Müller, A. M. K. *Phys. Lett.* **1984**, *105A*, 446.
(61) Fulton, R. L. *J. Phys. Chem. A* **2004**, *108*, 11691.
(62) Fulton, R. L.; Mixon, S. T. *J. Phys. Chem.* **1993**, *97*, 7530.
(63) Fulton, R. L.; Mixon, S. T. *J. Phys. Chem.* **1995**, *99*, 9768.
(64) Fulton, R. L.; Perhacs, P. *J. Phys. Chem. A* **1998**, *102*, 8988.
(65) Luken, W. L.; Beratan, D. N. *Theor. Chem. Acc.* **1982**, *61*, 265.
(66) Luken, W. L.; Culberson, J. C. *Theor. Chem. Acc.* **1984**, *66*, 279.
(67) Wang, J.; Smith, V. H., Jr. *Int. J. Quant. Chem* **1995**, *56*, 509.
(68) Tschinke, V.; Ziegler, T. *J. Chem. Phys.* **1990**, *93*, 8051.
(69) Sperber, G. *Int. J. Quant. Chem.* **1971**, *5*, 189.
(70) Ponec, R. *J. Math. Chem.* **1997**, *21*, 323.
(71) Ponec, R. *J. Math. Chem.* **1998**, *23*, 85.
(72) Ponec, R.; Yuzhakov, G.; Carbó-Dorca, R. *J. Comput. Chem* **2003**, *24*, 1829.
(73) Geier, J. *J. Phys. Chem. A* **2006**, *110*, 9273.
(74) Koga, T.; Nii, Y.; Matsuyama, H. *J. Phys. B: At. Mol. Opt. Phys.* **2000**, *33*, 2775.
(75) Koga, T. *J. Mol. Struct. (Theochem)* **2000**, *527*, 1.
(76) Koga, T.; Matsuyama, H. *J. Phys. B: At. Mol. Opt. Phys.* **1998**, *31*, 3765.
(77) Thakkar, A. J.; Tripathi, A. N.; Smith, V. H., Jr. *Int. J. Quant. Chem.* **1984**, *26*, 157.
(78) Coleman, A. J. *Int. J. Quant. Chem. Symp. 1* **1967**, 457.
(79) Cioslowski, J.; Liu, G. *J. Chem. Phys.* **1996**, *105*, 8187.
(80) Cioslowski, J.; Liu, G. *J. Chem. Phys* **1999**, *110*, 1882.
(81) Cioslowski, J.; Liu, G.; Rychlewski, J.; Cencec, W.; Komasa, J. *J. Chem. Phys.* **1999**, *111*, 3401.
(82) Fradera, X.; Duran, M.; Mestres, J. *J. Phys. Chem. A* **2000**, *104*, 8445.
(83) Sarasola, C.; Dominguez, L.; Aguado, M.; Ugalde, J. M. *J. Chem. Phys.* **1992**, *96*, 6778.
(84) Fradera, X.; Duran, M.; Mestres, J. *J. Chem. Phys.* **1997**, *107*, 3576.
(85) Thakkar, A. J.; Tripathi, A. N.; Smith, V. H., Jr. *Phys. Rev. A* **1984**, *29*, 1108.
(86) Tripathi, A. N.; Smith, V. H., Jr.; Thakkar, A. J. *Int. J. Quant. Chem.* **1989**, *35*, 869.
(87) Wang, J.; Tripathi, A. N.; Smith, V. H., Jr. *J. Chem. Phys* **1994**, *101*, 4842.
(88) Tschinke, V.; Ziegler, T. *Can. J. Chem.* **1989**, *67*, 460.
(89) Gunnarsson, O.; Jonson, M.; Lundqvist, B. I. *Phys. Rev. B* **1979**, *20*, 3136.
(90) Becke, A. D. *Int. J. Quant. Chem* **1983**, *23*, 1915.
(91) Schmider, H.; Edgecombe, K. E.; Smith, V. H., Jr.; Weyrich, W. *J. Chem. Phys.* **1992**, *96*, 8411.
(92) Schmider, H.; Smith, V. H., Jr. *Theor. Chem. Acc.* **1993**, *86*, 115.
(93) Gadre, S. R.; Kulkarni, S. A.; Pathak, R. K. *Phys. Rev. A* **1989**, *40*, 4224.
(94) Schmider, H. *J. Chem. Phys.* **1996**, *105*, 11134.
(95) Kadantsev, E. S.; Schmider, H. L. *Int. J. Quant. Chem.* **2008**, *108*, 1.
(96) Glendening, E. D.; Weinhold, F. *J. Comput. Chem.* **1998**, *19*, 593.
(97) Herges, R.; Geuenich, D. *J. Phys. Chem. A* **2001**, *105*, 3214.
(98) Program keywords: int(grid=ultrafine), scf=tight, opt=verytight.
(99) Frisch, M. J.; Trucks, G. W.; Schlegel, H. B.; Scuseria, G. E.; Robb, M. A.; Cheeseman, J. R.; Montgomery, J. A., Jr.; Vreven, T.; Kudin, K. N.; Burant, J. C.; Millam, J. M.; Iyengar, S. S.; Tomasi, J.; Barone, V.; Mennucci, B.; Cossi, M.; Scalmani, G.; Rega, N.; Petersson, G. A.; Nakatsuji, H.; Hada, M.; Ehara, M.; Toyota, K.; Fukuda, R.; Hasegawa, J.; Ishida, M.; Nakajima, T.; Honda, Y.; Kitao, O.; Nakai, H.; Klene, M.; Li, X.; Knox, J. E.; Hratchian, H. P.; Cross, J. B.; Adamo, C.; Jaramillo, J.; Gomperts, R.; Stratmann, R. E.; Yazyev, O.; Austin, A. J.; Cammi, R.; Pomelli, C.; Ochterski, J. W.; Ayala, P. Y.; Morokuma, K.; Voth, G. A.; Salvador, P.; Dannenberg, J. J.; Zakrzewski, V. G.; Dapprich, S.; Daniels, A. D.; Strain, M. C.; Farkas, O.; Malick, D. K.; Rabuck, A. D.; Raghavachari, K.; Foresman, J. B.; Ortiz, J. V.; Cui, Q.; Baboul, A. G.; Clifford, S.; Cioslowski, J.; Stefanov, B. B.; Liu, G.; Liashenko, A.; Piskorz, P.; Komaromi, I.; Martin, R. L.; Fox, D. J.; Keith, T.; Al-Laham, M. A.; Peng, C. Y.; Nanayakkara, A.; Challacombe, M.; Gill, P. M. W.; Johnson, B.; Chen, W.; Wong, M. W.; Gonzalez, C.; Pople, J. A. *Gaussian 03W, version 6.0, revision B.04*; Gaussian Inc.: Pittsburgh PA, 2003.
(100) Frisch, A.; Frisch, M. J.; Trucks, G. W. *Gaussian 03 User's Reference, Second Edition*; Gaussian Inc.: Wallingford (USA), 2005.
(101) Flükiger, P.; Lüthi, H. P.; Portmann, S.; Weber, J. *Molekel, version 4.3*; Swiss Centre for Scientific Computing: Manno (Switzerland), 2002.
(102) Popelier, P. L. A. *Mol. Phys.* **1996**, *87*, 1169.
(103) Sloan, I. H.; Womersley, R. S. *Adv. Comput. Math.* **2004**, *21*, 107.
(104) Sloan, I. H.; Womersley, R. S. *J. Comput. Appl. Math.* **2002**, *149*, 227.
(105) Péres-Jordá, J. M.; Becke, A. D.; San-Fabián, E. *J. Chem. Phys.* **1994**, *100*, 6520.
(106) Biegler-König, F.; Schönbohm, J. *AIM 2000, version 2.0*; Büro für Innovative Software C. Streibel Biegler-König: Bielefeld (Germany), 2002.
(107) Biegler-König, F.; Schönbohm, J. *J. Comput. Chem.* **2002**, *23*, 1489.
(108) Eskandari, K.; Mandado, M.; Mosquera, R. A. *Chem. Phys. Lett.* **2007**, *437*, 1.
(109) This is possible because in planar **6** all elements of the atomic overlap matrix between σ and π orbitals are zero.
(110) The nonadjacent monoionic[111,112] structure IV has actually rather low weight.[50,113,114] Although 1,4-delocalization is frequently represented by IV, the contribution of the corresponding diionic structure III is more important.
(111) Maynau, D.; Said, M.; Malrieu, J. P. *J. Am. Chem. Soc.* **1983**, *105*, 5244.
(112) Malrieu, J. P.; Maynau, D. *J. Am. Chem. Soc.* **1982**, *104*, 3021.
(113) Hiberty, P. C.; Ohanessian, G. *Int. J. Quant. Chem.* **1985**, *27*, 259.
(114) Bachler, V. *J. Comput. Chem.* **2004**, *25*, 343.
(115) Shurki, A.; Hiberty, P. C.; Dijkstra, F.; Shaik, S. *J. Phys. Org. Chem.* **2003**, *16*, 731.
(116) Ionic resonance structures like A^-B^+ and A^+B^- contribute to the π electron populations of A and B, but not to the π electron pair population between A and B. Their inclusion into an N-electron distribution, which is dominated by structures containing simultaneously electrons at A and B (like I), lowers the actual number of pairs relative to the product of electron populations, i.e. introduces negative correlation (cf. $\Gamma_X(\mathbf{r}_1,\mathbf{r}_2)$ in 1).
(117) Calculated from the two occupied π molecular orbitals perpendicular to the molecular plain.
(118) Cremer, D.; Reichel, F.; Kraka, E. *J. Am. Chem. Soc.* **1991**, *113*, 9459.
(119) Ref.73. The use of B3LYP instead of HF orbitals causes no significant qualitative differences.

JP800202W